Properties of epitaxial graphene grown on C-face SiC compared to Si-face

Leif I Johansson and Chariya Virojanadara

Original Publication:

Leif I Johansson and Chariya Virojanadara, Properties of epitaxial graphene grown on C-face SiC compared to Si-face, 2014, Journal of Materials Research, (29), 3, 426-438.
http://dx.doi.org/10.1557/jmr.2013.261

Properties of epitaxial graphene grown on C-face SiC compared to Si-face

Leif I. Johansson[a)] and Chariya Virojanadara[b)]
Department of Physics, Chemistry and Biology, Linköping University, SE-58183 Linköping, Sweden

(Received 25 June 2013; accepted 26 August 2013)

Epitaxial graphene of uniform thickness prepared on SiC is of great interest for various applications. On the Si-face, large area uniformity has been achieved, and there is a general consensus about the graphene properties. A similar uniformity has yet not been demonstrated on the C-face where the graphene has been claimed to be fundamentally different. A rotational disorder between adjacent graphene layers has been reported and suggested to explain why multilayer C-face graphene show the π-band characteristic of monolayer graphene. Utilizing low energy electron microscopy, x-ray photoelectron electron microscopy, low energy electron diffraction, and photoelectron spectroscopy, we investigated the properties of C-face graphene prepared by sublimation growth. We observe the formation of micrometer-sized crystallographic grains of multilayer graphene and no rotational disorder between adjacent layers within a grain. Adjacent grains are in general found to have different azimuthal orientations. Effects on C-face graphene by hydrogen treatment and Na exposure were also investigated and are reported. Why multilayer C-face graphene exhibits single layer electronic properties is still a puzzle, however.

I. INTRODUCTION

Graphene-based two-dimensional science and technology has developed into a new interdisciplinary area that has made a major impact on both fundamental and applied materials research. The current status of different graphene subfields and the wide range of graphene applications envisioned for the future are comprehensively described by the articles in the recent extended issue[1] of MRS Bulletin, "Graphene, fundamentals and functionalities." Graphene can be produced/grown using different methods,[1] but in this article, only properties of graphene grown epitaxially on the basal plane of the wide band gap semiconductor silicon carbide are discussed. This growth method is considered a most promising route[2–4] for the development of carbon nanoelectronics based on lithographic patterning of graphene. Large-scale epitaxial films with atomic layer-defined termination are highly desirable for electronic applications and also for fundamental studies of graphene functionalization. Methods to reliably grow high-quality graphene films with large-scale uniformity on SiC(0001), i.e., the Si-terminated surface, have been developed[4–8] but for the C-terminated SiC(000–1) surface graphene films[9–14] with similar large-scale uniformity has so far not been possible to produce.

Already in one of the earliest comparative studies[15] of the growth of carbon layers on the basal plane of 6H-SiC, it was reported that large single crystalline graphite layers could be obtained on the Si-face while the layers on the C-face had a significant polycrystalline character. The difference was then attributed[15] to a stronger interaction between the substrate and the small graphite patches, so they could not orient so freely, thereby inducing some azimuthal disorder of the patches that prevented the formation of a homogenous monolayer on the C-face. Later studies of epitaxial graphene grown on SiC also claimed[16–21] fundamental differences between C-face and Si-face graphene but provided a different explanation. A rotational disorder between adjacent graphene layers was reported for C-face graphene. Whereas Si-face graphene exhibits sharp low energy electron diffraction (LEED) spots and the Bernal (ABAB...) stacking, the macro LEED diffraction pattern obtained from C-face graphene is smeared out into a strongly modulated diffraction ring.[9,15,17,19,20] This, together with surface x-ray diffraction results,[16,17,20] was interpreted to indicate that the graphene layers on the C-face stack in such a way that adjacent layers are rotated with respect to each other. The experimental results indicated some preferred rotation angles and interleaved rotated layers. The rotational disorder produced moiré patterns in STM topographs[21] and was suggested to explain why epitaxial graphene films, tens of layers thick, show single layer electronic properties,[17,20] i.e., show a single π-band cone with the Dirac point located close to the Fermi level. Graphene on the C-face has therefore been called multilayer epitaxial graphene[3] and suggested to

Address all correspondence to these authors.
[a)]e-mail: lejoh@ifm.liu.se
[b)]e-mail: chavi@ifm.liu.se
This paper has been selected as an Invited Feature Paper.
DOI: 10.1557/jmr.2013.261

order azimuthally in a particular way with alternating 0 and 30° rotations of the layers relative to the SiC substrate. Such a stacking would not break the symmetry between the atoms in the unit cell and result in an electronic band structure of isolated/decoupled graphene layers. A set of nearly independent linearly dispersing bands would appear close to the $\bar{K}$ point in the graphene Brillouin zone, each originating from an individual rotated layer.[20] This is very different compared to the band structure of Si-face Bernal stacked graphene,[22] where only a single graphene layer gives rise to one π-band cone and linearly dispersing bands close to the $\bar{K}$ point. Bi- and trilayer graphene[22] give rise to two and three cones, respectively, and a nonlinear dispersion of the π-bands close to the $\bar{K}$ point.

Because of these reported fundamental differences between C-face and Si-face graphene, we studied graphene samples grown on nominally on-axis C-face SiC, using mainly high temperature sublimation in an inert gas ambient but also lower temperature sublimation in high vacuum. The thickness, morphology, and electron band structure of the samples were investigated[11,14] using low energy electron microscopy (LEEM), x-ray photoelectron electron microscopy (XPEEM), conventional and selected area photoelectron spectroscopy (PES and micro-PES), selected area LEED (micro-LEED), and also conventional angle resolved photoelectron spectroscopy (ARPES). Our results showed formation of fairly large (some micrometer) grains (crystallographic domains) of graphene exhibiting sharp (1 × 1) spots in micro-LEED and adjacent grains with different azimuthal orientations. Selected area constant initial energy photoelectron angular distribution (PAD) patterns, $E_i(k_x,k_y)$, collected using XPEEM showed the same. When utilizing a small sampling area, one Dirac cone centered at each of the six $\bar{K}$ points in the Brillouin zone was clearly resolved. When using a large sampling area, several sets of such Dirac cones from differently oriented grains appeared giving rise to a ring-like pattern resembling the ring-like macro-LEED pattern. Our experimental results presented below clearly show the existence of fairly large graphene grains with different azimuthal orientations and that adjacent graphene layers, within such grains, are not rotationally disordered as earlier proposed for C-face graphene.

Intercalation of hydrogen has for Si-face graphene been shown[8,23–25] to be an efficient way to decouple the graphene from the substrate, transform the carbon buffer layer present on this surface, and thereby allow preparation of "quasi free-standing" large area samples of 1-monolayer (ML) and 2-ML graphene. Slightly p-doped monolayer graphene can be prepared[8] by intercalating samples on which only the buffer carbon layer has been grown. Since no investigation of hydrogen treatments of C-face graphene samples had been reported, a study was carried out[14] using a hydrogen treatment receipt earlier successfully applied to intercalate hydrogen on Si-face graphene samples. Effects of hydrogen intercalation were clearly revealed, as shown below but were found to have a detrimental effect on the graphene and not a positive effect as for Si-face graphene.

Besides hydrogen, several other elements do intercalate Si-face graphene, as reviewed in Ref. 8. Sodium, e.g., deposited on monolayer Si-face graphene intercalates[26–28] first between the carbon layers but with time also underneath the carbon buffer layer. Heating at temperatures around 100 °C promotes intercalation[26–28] but at higher temperatures Na starts to deintercalate and desorbs from the sample. The intercalation transforms the carbon buffer layer to a second graphene layer, as revealed by the appearance of a second π-band cone. The Dirac point is shifted downward by about 1.0 eV, showing that the graphene layers become strongly n-doped by the deposited Na. The effects induced by alkali metals on Si-face graphene have been investigated quite thoroughly, and there is a general consensus about these findings.[29–33] For graphene grown on C-face SiC, the situation is quite different. Only one π-band cone with the Dirac point located close to the Fermi level has in general been observed[20,34] even for multilayer graphene samples. Since C-face graphene forms in smaller domains/grains and thus have a higher density of defects on the surface Na can be assumed to intercalate in between the graphene layers and at the interface easier on C-face than on Si-face graphene. The idea was to see if similar effects would be induced by Na on C-face graphene after deposition and heating. The experimental findings,[35] presented below, show the Dirac point to shift downwards and the π-band to broaden considerably after Na deposition and heating, which can be interpreted to indicate intercalation in between the graphene layers.

II. MORPHOLOGY, STRUCTURE, AND STACKING

A. Si-face graphene

For comparison between graphene grown on C-face and Si-face SiC, some selected results[36] from a Si-face sample are shown in Fig. 1. This is a 1-ML graphene sample with 2-ML islands on it, and a typical LEEM image is shown in Fig. 1(a). Based on the observed variation[37] in the electron reflectivity with electron energy, one can immediately determine that the islands in the LEEM image correspond to 2 MLs and the brighter areas to 1-ML graphene. The field of view (FOV) in Fig. 1(a) is 20 μm. It deserves to be noted that Si-face samples where a homogenous coverage of 1-ML graphene is observed in LEEM images recorded at an FOV of 50 μm have been possible to prepare.[7] The selected area LEED diffraction patterns originating from the 1- and 2-ML areas in Figs. 1(b) and 1(c), respectively, show a distinct decrease in spot intensities around the main graphene spots for the 2-ML island. These additional spots originate from the first carbon layer formed on Si-face

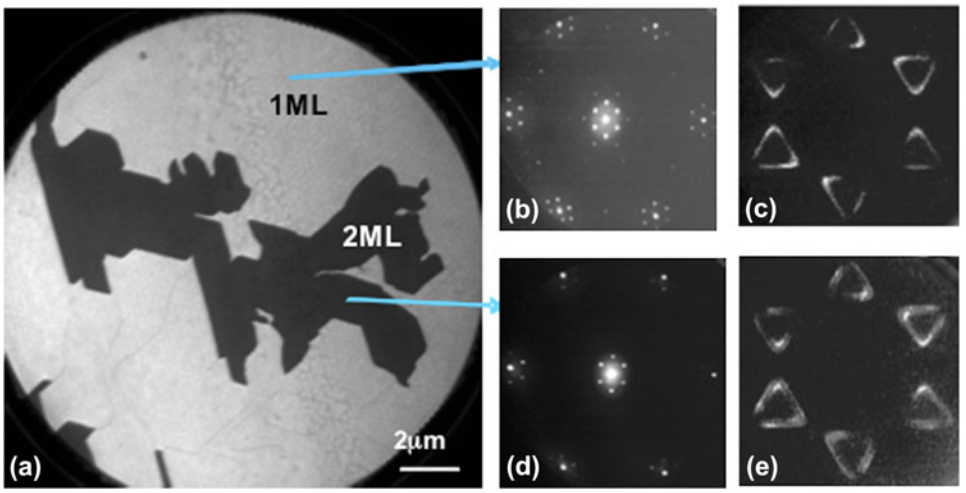

FIG. 1. (a) LEEM image collected from a furnace-grown 6H-SiC Si-face graphene sample at an FOV of 20 μm and an electron energy of 4.6eV. Micro-LEED patterns (400-nm probing area) recorded at 60 eV from (b) 1-ML and (c) 2-ML areas. High energy resolution PADs, $E_i(k_x,k_y)$, collected from (d) 1-ML and (e) 2-ML graphene areas at an initial energy, E_i, of 2.5 eV. Two π bands are clearly seen from the 2-ML areas.

SiC, the $6\sqrt{3} \times 6\sqrt{3}$R30° reconstructed buffer layer; so these patterns show that diffracted intensity is observed from at least three carbon layers at this electron energy. Diffraction patterns from different 1- and 2-ML areas look essentially identical all over the sample, only some variation in relative intensity between buffer layer spots is observed.[7] The buffer layer forms strong covalent bonds to the SiC substrate. It does not exhibit the electronic properties of graphene, i.e., shows no graphene π-band at the $\bar{K}$ point[19] and gives rise to an additional shifted component[19,38] in the C 1*s* core level spectrum. Selected area constant initial energy PAD patterns recorded[36] from the 1-ML or the 2-ML areas, respectively, are shown in Figs. 1(d) and 1(e). They were collected from a small (800 nm) area using XPEEM, a photon energy of 35 eV, and at an energy of 2.5 eV below the Fermi level. The six Dirac cones in the Brillouin zone are clearly revealed and seen to have a triangular shape at this energy of approximately 2 eV below the Dirac point. From the 2-ML island, the second π-band cone becomes clearly observable, see Fig. 1(e), in this data set that was taken at the highest possible instrument energy resolution (~0.15 eV). When using photons in this energy range, contribution from three to four graphene layers can[22] typically be distinguished. For the graphene forming on the Si-face, a single π-band (cone) with linear dispersion at the $\bar{K}$ point results[39] only for single layer graphene, whereas bi- and trilayer graphene show[39,40] two and three split parabolic π-bands (cones) at the $\bar{K}$ point, respectively. If the two layers on the 2-ML islands instead would be decoupled, i.e., behave as independent single layers of graphene as suggested for multilayer C-face graphene, and moreover be rotated azimuthally relative to each other by an angle different than 60° × integer, one would in Fig. 1(e) see two sets of these six Dirac cones rotated relative to each other by exactly that angle. In selected area LEED, not only two rotated (1 × 1) patterns would then be seen but also characteristic additional diffraction spots, originating from the sum and difference between the two sets of reciprocal lattice vectors, would appear.[41] Thus, both in selected area LEED patterns and selected area PAD images, it is possible to directly reveal if adjacent graphene layers are rotationally disordered, i.e., if they are rotated azimuthally relative to each other by an angle different than 60° × integer.

B. C-face graphene

Results from three different C-face graphene samples, all grown at high sublimation temperature and in an Ar ambient, are presented for the purpose to illustrate typical results concerning surface morphology, structure, and stacking and differences compared to Si-face samples. A LEEM image collected from one 6H-SiC C-face graphene sample at an electron energy of 3.3 eV and an FOV of 10 μm is shown in Fig. 2(a). The electron reflectivity versus electron kinetic energy curve, i.e., the so-called I(V) curve, extracted from the areas labeled from A to P are shown in Fig. 2(b). Curves A to I are very similar and show two pronounced minima that indicate 2-ML graphene. Curves J to N also show two minima indicating a coverage of 2 MLs, although these curves have a slightly different shape around 2 eV than curves A to I. Curve O shows one dip indicating monolayer graphene, and curve P represents an area with no graphene coverage. Most of the surface of this sample has a graphene coverage of 2 MLs. Selected area LEED patterns collected from areas E and D at an energy of 45 eV are shown in Fig. 2(c). A probing area with a diameter of 0.4 μm was used, so that both patterns are collected from a single grain/domain, and the two domains are seen to have

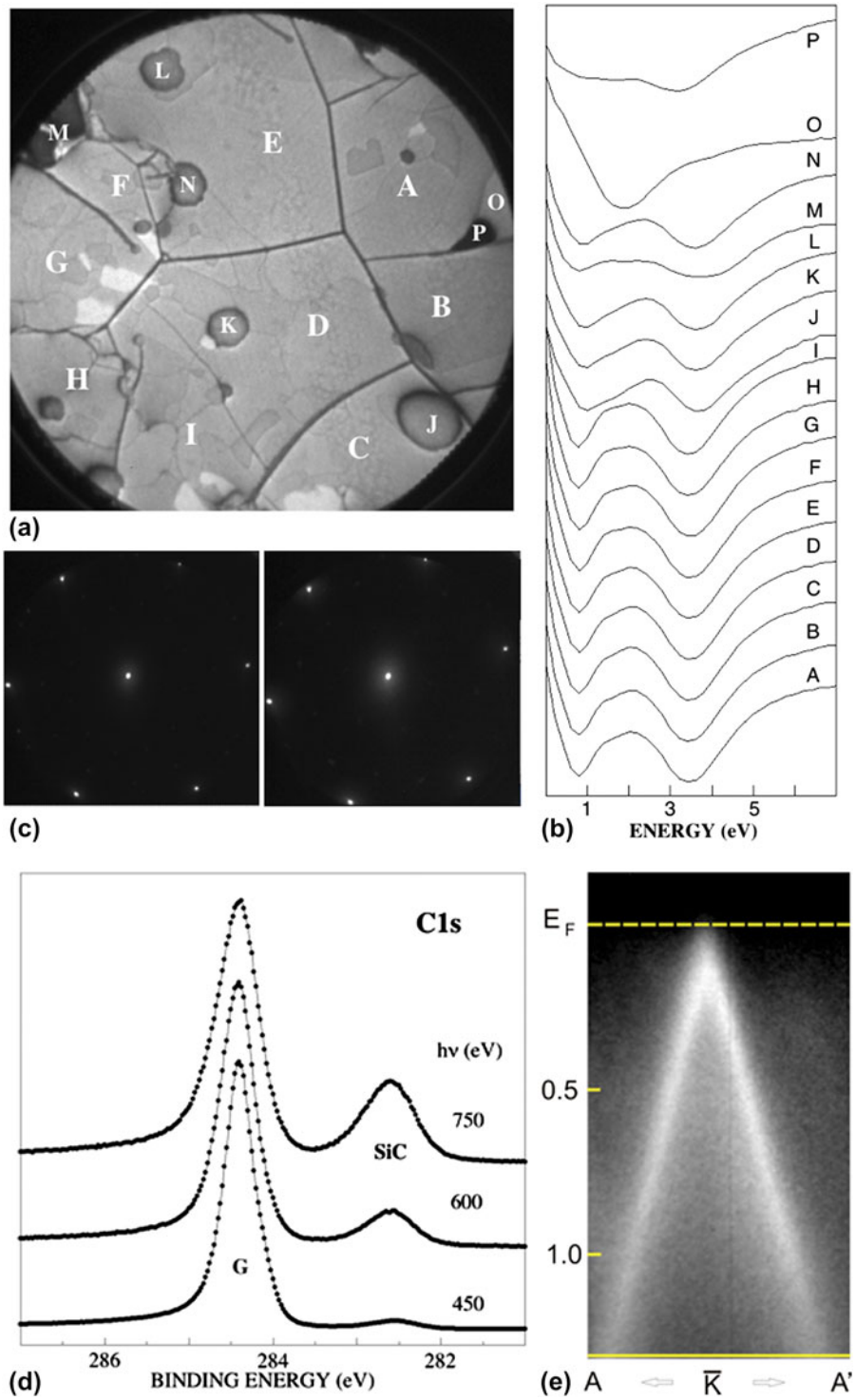

FIG. 2. (a) LEEM image recorded from a 6H-SiC C-face graphene sample at 0.4 eV and an FOV of 10 μm. (b) I(V) curves extracted from the different areas labeled A to P in (a), showing a coverage of mainly 2 MLs of graphene. (c) Micro-LEED patterns, collected at 45 eV using a probing area diameter of 400 nm, from two different grains/domains in (a). (d) C 1*s* spectrum recorded using three different photon energies showing contribution from graphene (G) and the SiC substrate. (e) The π-band recorded around the $\bar{K}$ point using a photon energy of 33 eV.

different azimuthal orientations. C 1*s* spectra collected, using conventional macro-PES, from this "2-ML" graphene sample at three photon energies are shown in Fig. 2(d). They are modeled accurately using only two components, the SiC component from the substrate and the G component from the graphene layers. In agreement with

earlier results,[11,19] no trace of a carbon buffer layer component can be observed. The energy separation of 1.9 eV and peak intensity ratio of around 6 (at 600 eV) determined between the graphene and the SiC components (G/SiC) are consistent with previously determined values[19] for a graphene thickness of about 2 MLs. The π-band recorded, using conventional macro-ARPES, from this 2-ML graphene sample around the $\bar{K}$ point and along the A–$\bar{K}$–A' direction using a photon energy of 33 eV is shown in Fig. 2(e). The Dirac point is located within approximately 75 meV below the Fermi level indicating a slight n-doping instead of the slight p-doping earlier reported.[34] Since the graphene grain size was only on the order of a few micrometers, a few π-cones from domains of different azimuthal orientations were typically detected when moving the light spot over the sample. However, the Dirac point of the different cones appeared always located at the same energy position.

An LEEM image collected from a 4H-SiC C-face sample at 1.3 eV and an FOV of 10 μm is shown in Fig. 3(a). The extracted reflectivity curves from the areas labeled 1–8, respectively, in Fig. 3(b) show that several of them have the same number of graphene layers. Six minima are clearly observed in curves 1, 2, 6, 7, and 8, whereas curves 3, 4, and 5 at first appear to have only five minima. However, when looking in detail at these latter three curves, one finds that there actually appears a weak minimum at around 6.5 eV. The coverage may be 6 MLs over the whole area in Fig. 3(a), but if some areas actually have 5 MLs is not important for the main message contained in Figs. 3(c) and 3(d). The selected area LEED patterns collected using a probing area of 400 nm from the positions labeled 1 and 2 in Fig. 3(a) are shown in the two upper panels in Fig. 3(c). It is obvious from these LEED patterns that a grain size larger than 400 nm has been accomplished on this sample and that the stacking of the six graphene layers is such that adjacent layers are not rotated with respect to each other. The third, bottom, panel in Fig. 3(c) shows the LEED pattern collected using a 5-μm large probing area at position 2. The sampled area then includes domains 2 and 1, and it is obvious that two grains of different azimuthal orientations are now probed since this LEED pattern just represents a superposition of the patterns shown in the upper two panels. The characteristic additional diffraction spots,[41] originating from rotated/twisted layers are not discernable. To further emphasize that grains of six layers of graphene can form on the C-face and be stacked in such a way that no rotational disorder exists between adjacent layers, some PADs of the π-band were also recorded. Two such patterns collected using a probing area of 800 nm, a photon energy of 45 eV, and at an energy of about 2 eV below the Fermi energy are shown in Fig. 3(d). Only six Dirac cones, which appear triangular at this initial energy centered around the six $\bar{K}$ points in the Brillouin zone are observed in these

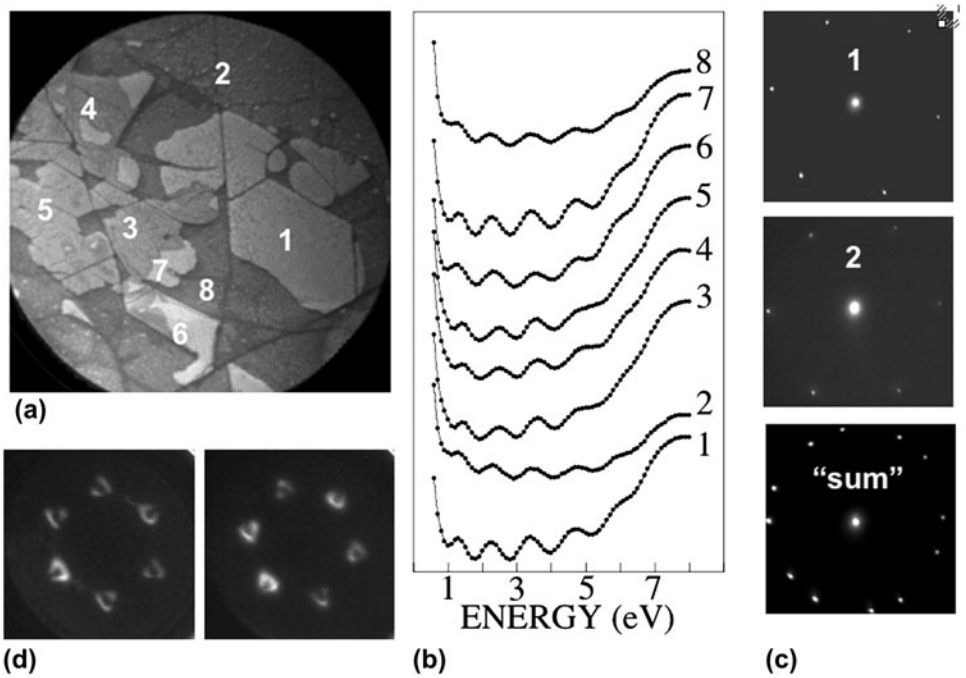

FIG. 3. (a) LEEM image recorded from a 4H-SiC C-face graphene sample at 1.3 eV and an FOV of 10 μm. (b) Electron reflectivity curves extracted from different areas labeled 1–8. (c) The two upper panels show selected area LEED patterns collected at 45 eV using a probing area of 400 nm from the positions labeled 1 and 2 in Fig. 3(a). The lower panel shows the LEED pattern collected using a 5-μm aperture at position 2. (d) Shows two constant initial energy PAD patterns, $E_i(k_x,k_y)$, of the π-band collected using a probing area of 800 nm, a photon energy of 45 eV, and at an energy of about 2 eV below the Fermi level. One Dirac cone centered around each of the six $\bar{K}$ points in the Brillouin zone is clearly observed.

patterns. They were collected at two different locations outside the area shown in Fig. 3(a) but where the number of graphene layers was also six. These patterns show clearly that well ordered grains of multilayer graphene larger than 800 nm has formed and that adjacent graphene layers are not rotated relative to each other. At this photon energy, separate and distinguishable signals from three to four layers of graphene have been demonstrated from Si-face samples.[22] Moreover, the PAD patterns recorded[36] from bilayer graphene show two π-cones of fairly similar intensity centered around each $\bar{K}$ point so any rotational disorder present between the two and three uppermost graphene layers would show up directly in these patterns. The two patterns, in Fig. 3(d), show that the different grains probed do have different azimuthal orientations. It should be noted that when selecting a larger probing area that included two grains of different azimuthal orientations, two sets of superimposed Dirac cones were detectable, just similar to the two superimposed micro-LEED patterns shown in the bottom panel in Fig. 3(c).

Two LEEM images from different locations of another C-face graphene sample are shown in Figs. 4(a) and 4(c). These images were collected at an FOV of 25 μm and energies of 3.9 and 5.1 eV, respectively. Several different domains are clearly visible, and the I(V) curves extracted from the different domains, displayed in Figs. 4(b) and 4(d), show the number of graphene layers present. The lightest gray areas in Fig. 4(a) have a graphene coverage of 1 ML, whereas some other areas have thicknesses of 4 MLs and 5 MLs of graphene. In Fig. 4(c), the light gray areas have a coverage of 2 MLs. The other I(V) curves, labeled A, B, C, D, and E, do not show similarly well-defined modulations in the reflectivity and indicate areas where a mixture of different numbers of graphene layers probably exist. The really dark areas in both Figs. 4(a) and 4(c) showed no graphene coverage but the presence of an ordered silicate, observed and discussed earlier.[9–13] However, the important point here is that large enough areas of 1 ML, 2 MLs, and 4 MLs of graphene were identified by LEEM, so selected area PES, LEED, and XPEEM could be applied. Selected area C 1*s* spectra collected using a photon energy of 450 eV and a probing area of 4 μm are displayed in Fig. 5(a). Contribution from the SiC substrate is clearly resolved, at around 1.9 eV lower binding energy than the graphene component, in the spectra from the 1-ML and 2-ML areas but is not discernible from areas having 4-ML graphene. These C 1*s* spectra show no hint of a dense disordered carbon interface layer, which earlier has been proposed to be present, at least locally.[10,13] Selected area LEED patterns collected using two different electron energies from the three areas with different graphene coverage are shown in Figs. 5(b)–5(g). A probing area of 1.5 μm was utilized, so the pattern is in each case collected from a single crystallographic grain having a specific number of graphene layers. The patterns collected at 45 eV, Figs. 5(b), 5(d), and 5(f), all show distinct (1 × 1) patterns and no presence of additional superstructure spots. When increasing the energy to 145 eV, additional weaker spots, of which three are marked by white circles, are possible to be observed in the patterns from the 1-ML and 2-ML areas, whereas such spots are not visible in the pattern from the 4-ML area. These weaker spots are interpreted to originate from the SiC substrate, since the (1 × 1) diffraction spots from the SiC substrate and graphene appear at the same distances, within the experimental uncertainty, for graphene grown on Si-face SiC, as can be seen in Fig. 1(b). There, the substrate spots are always rotated 30° relative to the graphene (1 × 1) spots, and although the angle is close to 30°, also in this case, we observed at other locations and for other samples a different angle. No additional superstructure spots originating from rotated graphene layers are thus observed in any of the micro-LEED patterns in Fig. 5. To further demonstrate that the graphene layers are stacked in such a way that no rotational disorder exists between

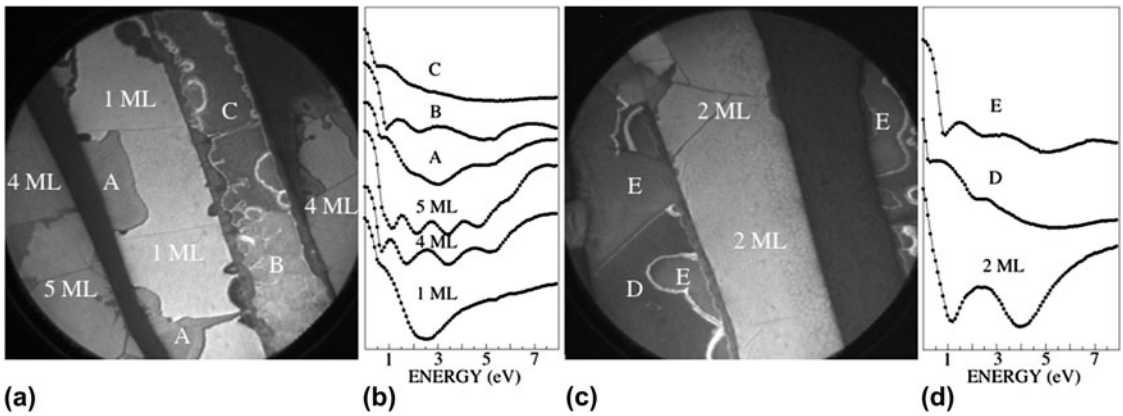

FIG. 4. LEEM images collected at an FOV of 25 μm from a 6H-SiC C-face graphene sample using an energy of (a) 3.9 eV and from another position (c) at an energy of 5.1 eV. The I(V) curves in (b) and (d), extracted from different locations in (a) and (c) respectively, reveal fairly large areas of 1, 4, and 5 MLs and 2 MLs of graphene.

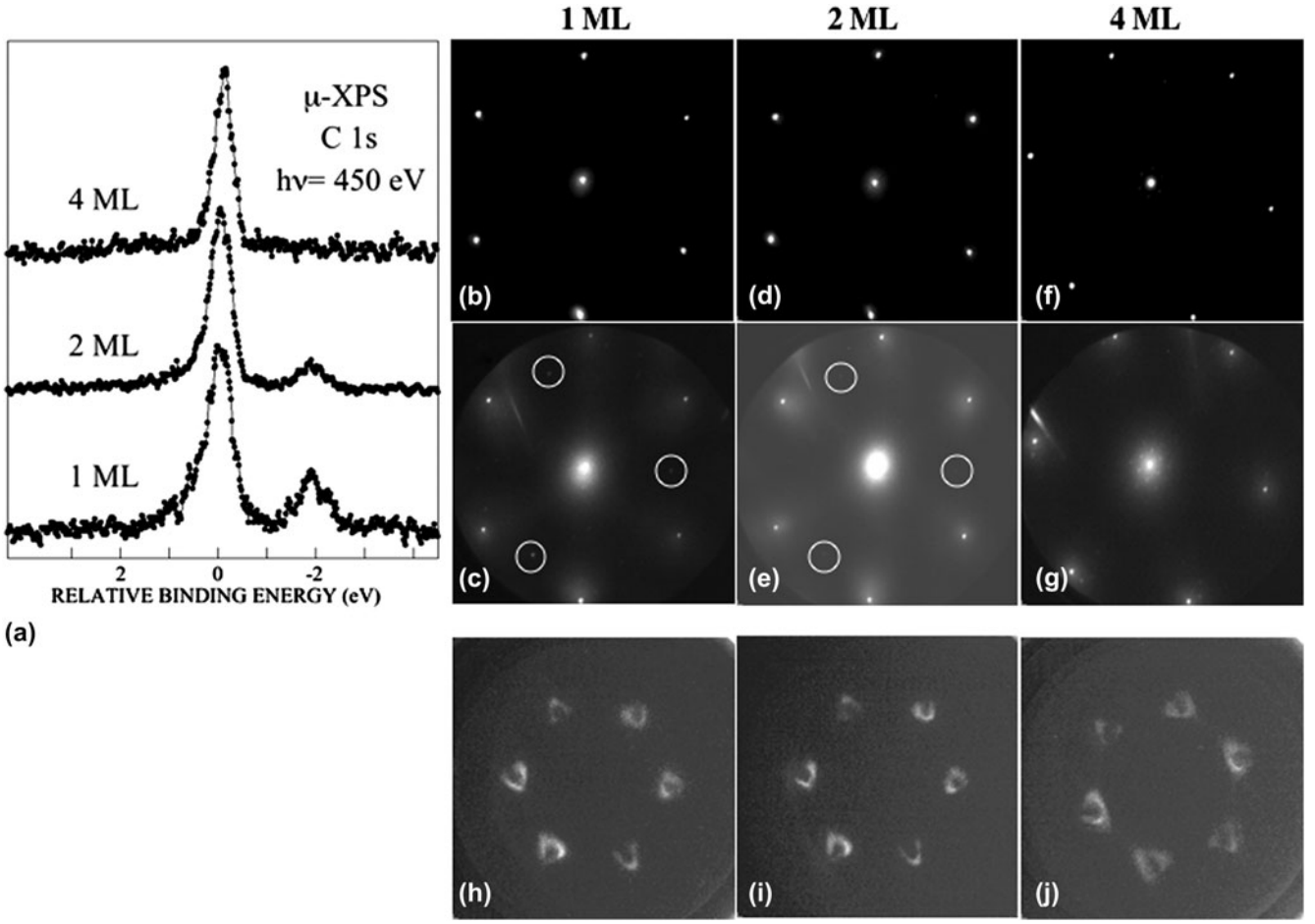

FIG. 5. (a) C 1*s* spectra collected, using a probing area of 4 μm, from the marked areas in Fig. 4 with different numbers of graphene layers. (b)–(g) show 1.5-μm selected area LEED patterns from: the 1-ML area at (b) 45 eV and (c) 145 eV; the 2-ML area at (d) 45 eV and (e) 145 eV; and the 4-ML area at (f) 45 eV and (g) 130 eV, respectively. In (h)–(j), PADs, $E_i(k_x,k_y)$, recorded from, respectively, the 1-ML, 2-ML, and 4-ML areas are shown. The PADs were collected at 1.5 eV below the Fermi level, using a probing area of 800 nm.

adjacent layers, recorded PADs of the π-band from areas with a different numbers of graphene layers are shown in Figs. 5(h)–5(j). These patterns were collected using a probing area of 800 nm, a photon energy of 45 eV, and at an energy of about 1.5 eV below the Fermi energy. Only six Dirac cones, centered around the six $\bar{K}$ points in the Brillouin zone are observed. The patterns thus show clearly that well-ordered grains of multilayer graphene larger than 800 nm have formed and that adjacent graphene layers within these grains are not rotated relative to each other.

C. Hydrogen-treated C-face graphene

Intercalation of hydrogen of Si-face graphene has been quite thoroughly studied,[8,23–25] but no investigation of hydrogen intercalation of C-face graphene had been reported. Therefore, a receipt earlier successfully applied[42] to intercalate hydrogen on Si-face graphene samples was utilized, i.e., heating in a pure hydrogen ambient at 700 °C, to treat C-face graphene samples and study the effects. A LEEM image, collected at 1.7 eV and an FOV of 50 μm, from a C-face sample grown by sublimation at a high temperature in an argon atmosphere, is shown in Fig. 6(a). It is a representative image of the surface morphology, since similar images were obtained at other positions on this sample. After hydrogen treatment, the LEEM images obtained were distinctly different, as illustrated by the representative image in Fig. 6(b). The domain structure clearly observed on the as-grown sample has more or less disappeared after hydrogen treatment, and considerably smaller domains and contrast variations are observed. For the as-grown sample, in Fig. 6(a), I(V) curves showing pronounced periodic variations indicating a coverage of mainly 3 and 4 MLs of graphene were extracted. For the hydrogen-treated sample, Fig. 6(b), extracted I(V) curves also showed periodic variations but considerably less pronounced. Selected area LEED patterns collected appeared clear and distinct but were found to change with time when using the typical micro-LEED electron beam current of 200 nA. The beam actually produced changes on the surface that were clearly detectable by LEEM after

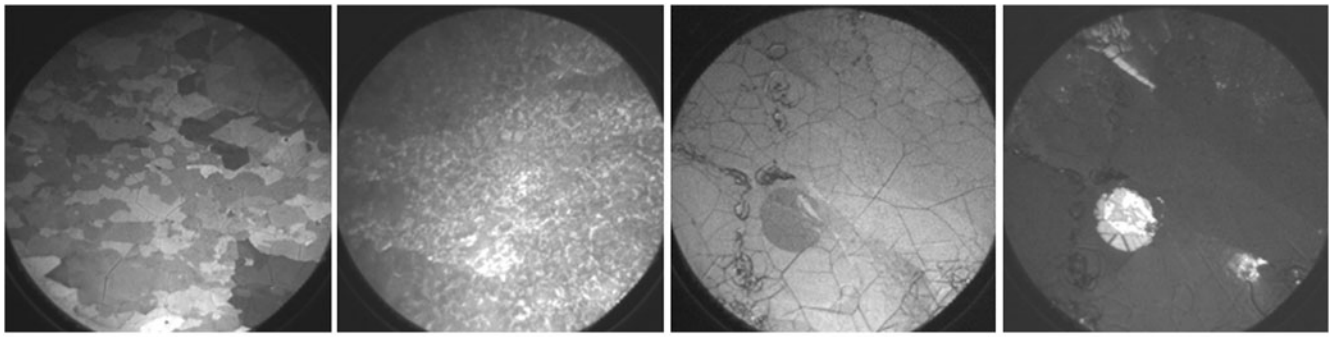

FIG. 6. LEEM images collected from a 6H-SiC C-face graphene sample at 1.7 eV and an FOV of 50 μm: (a) as-grown and (b) after hydrogen treatment. The images in (c) and (d) were collected at an FOV of 25 μm from another hydrogen-treated sample at energies of 1.7 and 6.5 eV, respectively. The circular dark and bright spot seen in (c) and (d) was created by electron beam illumination during collection of micro-LEED patterns.

only a few minute exposure, as illustrated in Figs. 6(c) and 6(d). This hydrogen-treated sample was initially grown by sublimation at a lower temperature and in high vacuum and can then be expected to initially have smaller graphene grains/domains. For Si-face graphene, it is well known that sublimation growth at lower temperatures and in high vacuum result in significantly smaller domains than at high temperature and in an Ar ambient. With more grain boundaries and thus defects present on the surface, the effects of hydrogen exposures can be expected to be larger. This sample was deliberately exposed to the typical micro-LEED electron beam current over an area with a radius of approximately 5 μm for about 2 min. The illuminated circular area appears darker and brighter in the LEEM images in Figs. 6(c) and 6(d) that were collected at an FOV of 25 μm and energies of 1.7 and 6.5 eV, respectively. This clearly demonstrates that the typical micro-LEED electron beam current does induce changes in hydrogen-treated C-face graphene samples, and hydrogen desorption appears to be the most likely reason. Before looking at how the micro-LEED pattern typically changed with time, it deserves to be mentioned that for this hydrogenated sample, in Figs. 6(c) and 6(d), the I(V) curves extracted outside the illuminated circular area did not show any periodic oscillations, but instead appeared similar to curve C in Fig. 4(b), irrespective of the size and position of the area selected. For this sample, the hydrogen treatment thus drastically affected the size of the domains and apparently also perturbed the periodicity in distance between the graphene sheets, since no interference effect was possible to observe in extracted reflectivity curves. Distinct changes in the micro-LEED pattern appeared rapidly, however. The pattern in Fig. 7(b) was recorded 2 min after that in Fig. 7(a) from the same spot of the hydrogen-treated sample. An energy of 45 eV and a probing area of 1.5 μm was selected, and this sample was the one initially prepared at low sublimation temperature and in high vacuum. The superstructure spots become clearly visible after only about 1 min of electron beam exposure. The strongest of the superstructure spots are marked by white circles in Fig. 7(b), and they are seen to have the same distance to the (0, 0) spot as the initial (1 × 1) graphene spots. In addition to these strong spots, there are other spots arranged in inner hexagonal patterns, like in the patterns recently reported[41] for specially prepared twisted bilayer graphene samples. When decreasing the micro-LEED electron beam current, to 10 nA, and moving to another spot on the sample, the pattern in Fig. 7(c) was obtained, which again is mainly a (1 × 1) graphene pattern. When increasing the electron beam current again, to 200 nA, the pattern in Fig. 7(d) resulted, which shows a similar set of six strong superstructure spots, although now at a different rotation angle. When increasing the electron energy to 80 and 142 eV, the same pattern remained, see Figs. 7(e) and 7(f); only the relative intensity between the main and superstructure spots is changed. These superstructure spots can be explained in the same way as earlier proposed[41] for twisted bilayer graphene samples, indicating a twist angle of around 35 and 20° in Figs. 7(b) and 7(d), respectively. Since this effect with electron beam exposure did not occur for the as-prepared graphene C-face samples, desorption of intercalated hydrogen appears as the most plausible explanation. Moreover, after local hydrogen desorption by electron beam illumination, the two uppermost graphene layers appear in general to be twisted relative to each other, which definitely was not the case on the large ordered grains on the as-prepared samples [see Figs. 2(c), 3(c), and 5(b)–5(g)]. Therefore, the hydrogen-treated sample was also heated in situ at 600 °C for a couple of minutes in an effort to desorb most of the hydrogen. The micro-LEED patterns collected afterward using the normal typical high electron current then showed no time effect. Stable (1 × 1) patterns, and also patterns containing superstructure spots similar to those in Fig. 7, were then obtained at different positions on the surface. However, extracted I(V) curves still did not show

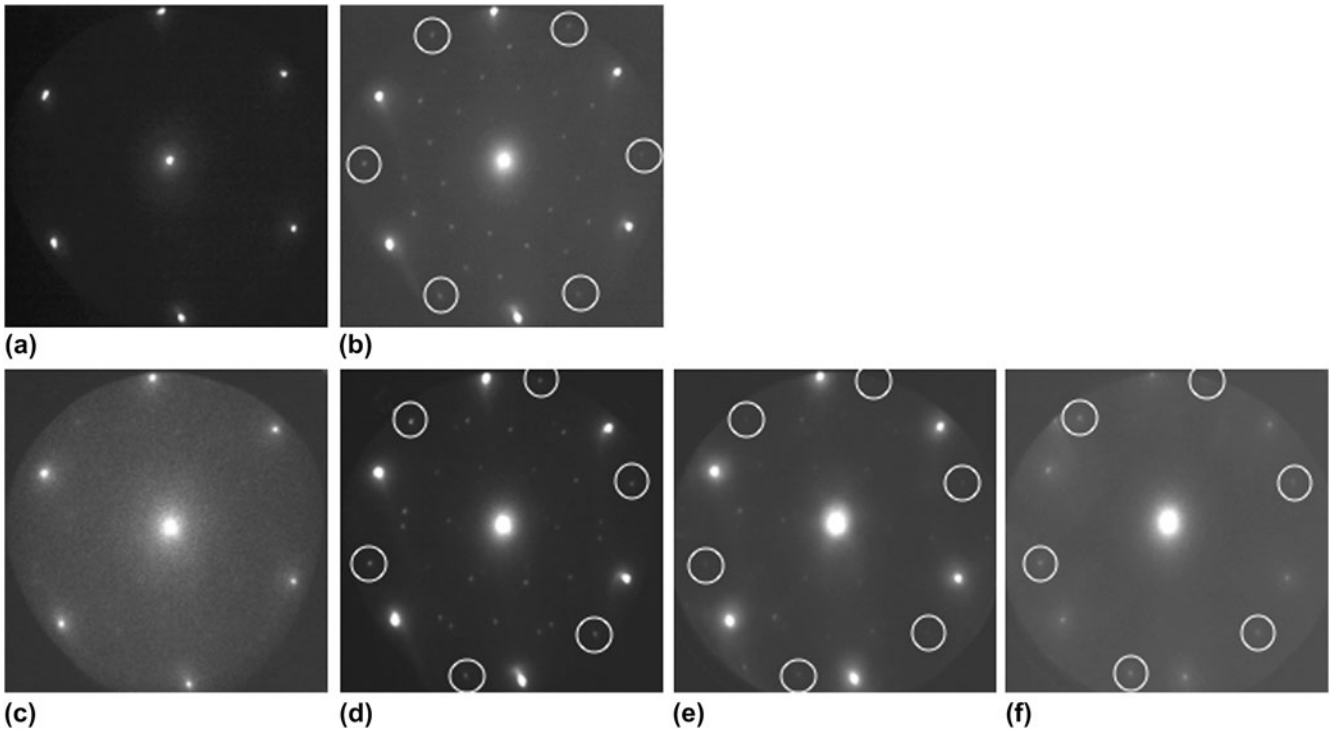

FIG. 7. (a) to (d) micro-LEED patterns recorded, from the hydrogenated sample shown in Figs. 6(c) and 6(d), using an energy of 45 eV and a probing area of 1.5 μm. The pattern was found to change from the (1 × 1) in (a) to that in (b), containing superstructure spots within a minute. When moving to another spot on the sample and using a low electron beam current, the (1 × 1) pattern in (c) was observed. When increasing to the normally used high electron beam current, the pattern in (d) appeared within a minute. The same pattern collected at (e) 80 eV and (f) 142 eV.

pronounced periodic variations; they still appeared similar to curve C in Fig. 4(b), irrespective of the size and position of the area selected. Before heating, selected area PES core level spectra were collected from the hydrogen-treated samples, both from areas previously illuminated and not illuminated by the LEED electron beam. No difference in the chemical composition between these areas could be revealed by the core-level spectra, which suggests local hydrogen desorption as the probable origin to the changes observed in the LEEM images in Figs. 7(c) and 7(d). A hydrogen treatment, which for Si-face graphene results in intercalation and improved properties, for C-face graphene instead results in deteriorated properties. The average grain/domain size is drastically reduced; adjacent graphene layers appeared for one sample to become decoupled, since no clear interference effect was observable in extracted I(V) curves, and after local hydrogen desorption by the electron beam, adjacent graphene layers are in general rotated relative to each other. Heat treatment of a hydrogenated C-face graphene sample did not restore the quality of the original as-grown sample; considerably smaller domain/grain sizes showing either (1 × 1) or twisted layer micro-LEED patterns were then observed. Thus, the hydrogen treatment tried for the C-face graphene samples had, contrary to the case for Si-face graphene, a detrimental effect on the quality and properties of the graphene.

D. Effects induced in the π-band structure by deposited sodium

The effects induced in the π-band structure close to the $\bar{K}$ point, after Na deposition and subsequent heating, were investigated[35] using conventional ARPES, on a C-face sample having predominantly 2-ML graphene coverage, actually the one presented in Fig. 2. After Na deposition, the Dirac point shifts down by about 0.5 eV, as shown in Fig. 8. Subsequent heating at 50 and 80 °C do not affect the band much, it only appears slightly more diffuse. Heating at temperatures from 120 to 300 °C results in a considerable broadening of the spectral features. At 400 °C, the Dirac point has moved back quite much toward E_F so most of the Na appears to have desorbed, and at 950 °C, the initial band is restored. An interesting thing is what causes the broader features that are observed particularly well at 200 and 300 °C. On Si-face graphene, intercalation of Na in between the carbon layers and also at the graphene SiC interface was strongly promoted[26–28] by heating at around 100 °C, whereas at higher temperatures, Na started to deintercalate and desorb from the surface, and therefore we suggest similar things to occur also on C-face graphene. After deposition and after heating at temperatures below approximately 100 °C, a large part of Na stays on the surface and in between the graphene layers. When heating at temperatures from 120 to 300 °C, intercalation at the

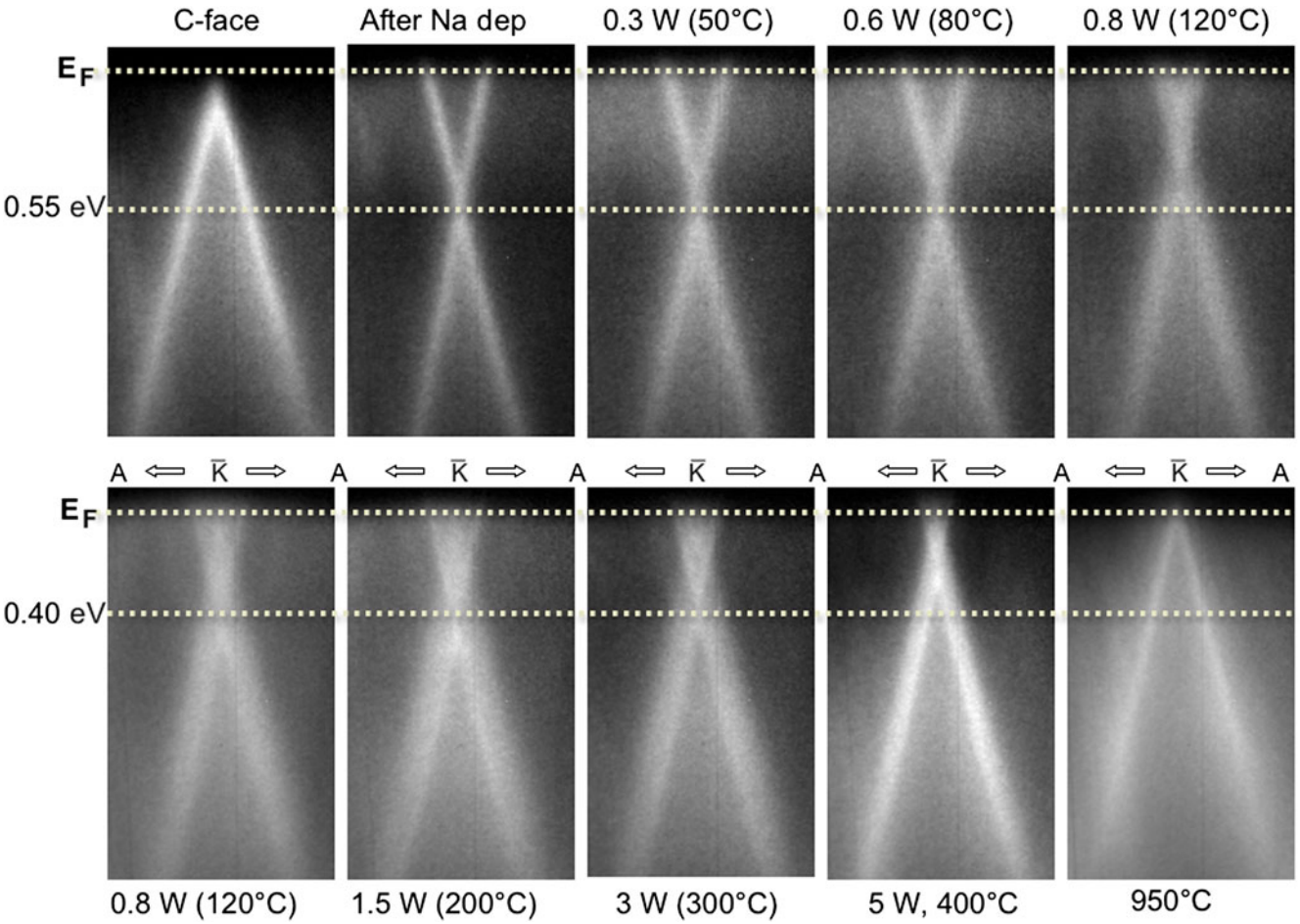

FIG. 8. The π-band structure recorded close to the $\overline{K}$ point along the A–$\overline{K}$–A' direction from the 6H-SiC C-face graphene sample shown in Fig. 2, using conventional ARPES, before and after Na deposition and after heating at different temperatures. A photon energy of 33 eV was used.

interface and in between the carbon layers is promoted, although the Na on the surface decreases considerably since Na begins to desorb. Then, the two carbon layers experience a different electron n-type doping level, so two π-bands, cones, are probably present, one with the Dirac point fairly close to E_F and the other with the Dirac point at around 0.4 eV below E_F. After heating at 400 °C, most of the Na has desorbed, but there is still some intercalated Na, giving rise to a smaller energy difference between the Dirac points of the two graphene layers. Intercalation at the interface can be unambiguously identified by the appearance[26,28] of shifted substrate components in the C 1*s* and Si 2*p* core-level spectra. However, on the beam line utilized for these band structure studies, the C 1*s* level was not accessible, but a limited set of Si 2*p* and Na 2*p* spectra was possible to collect, and they provided support[35] for the above speculations.

Since the Dirac point was shifted downwards from the Fermi level after Na deposition, it was possible to then investigate the band structure both above and below the Dirac point and compare with the band structure from the clean surface and with calculated results. For that purpose, $E_i(k_x,k_y)$ angular distribution patterns were extracted from the ARPES data collected around the $\bar{K}$ point at certain energies relative to the Dirac point. For the clean 2-ML graphene C-face sample, this pattern is a distinct small circular spot at E_D, see upper panel in Fig. 9 in which $E_i(k_x,k_y)$ patterns from the clean surface are displayed. When moving away from the Dirac point, the pattern has at 0.2 eV the shape of a circular ring which when moving further away becomes gradually more triangular. The intensity distribution and shape of these constant energy maps at and below the Dirac point agree well with the patterns calculated[43] for monolayer, but not bilayer, graphene. Close to the Dirac point, the calculated pattern for monolayer graphene is fairly circular, and when moving further away, it becomes more triangular due to the increased effect of triangular warping, as illustrated in Fig. 2 in Ref. 43. The asymmetry in the intensity distribution, the appearance of the so-called dark corridor,[44] has for monolayer graphene been well accounted for[43] by considering the two source interference patterns from the two inequivalent

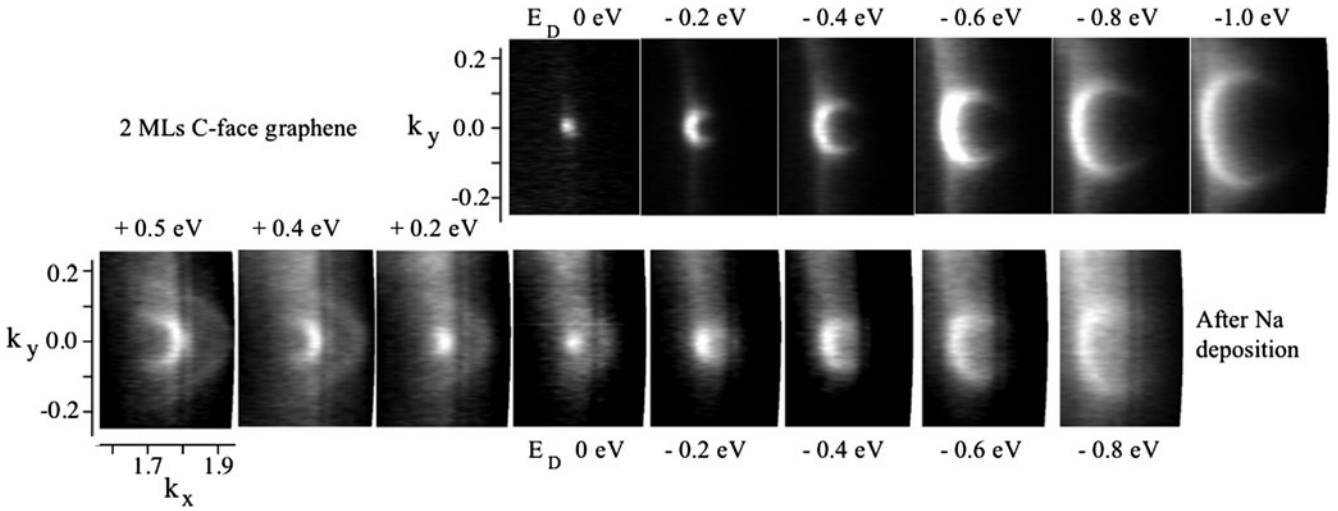

FIG. 9. PADs, $E_i(k_x,k_y)$, extracted around the $\overline{K}$ point from recorded ARPES spectra collected from the 6H-SiC C-face graphene sample before (upper panel) and after (lower panel) Na deposition. The wavevector k_x is along the $\overline{\Gamma} - \overline{K} - \overline{M}$ direction and k_y along A–$\overline{K}$–A'.

atomic sites in the graphene honeycomb lattice. After Na deposition, the patterns extracted below E_D appear fairly similar to those for the clean surface (see lower panel in Fig. 9). However, the circular spot at E_D is distinctly larger, and the patterns are slightly more diffuse but the doping has not induced any other visible changes in the symmetry of the pattern. When looking at the patterns extracted above E_D, they are flipped, "mirrored," compared to the pattern at the same energy below E_D. This was also predicted at energies located above E_D for monolayer graphene, as shown in Fig. 2 in Ref. 43, but not for Bernal stacked bilayer graphene. Thus, both for the as-grown 2-ML graphene C-face sample and for the doped graphene after Na deposition, the $E_i(k_x,k_y)$ angular distribution patterns extracted reflect those predicted for monolayer graphene, whereas the patterns predicted for Bernal stacked bilayer graphene look distinctly different, especially at energies below the Dirac point, as shown in Fig. 4 in Ref. 43. It is thus clear that the two graphene layers on our as-grown C-face sample are not Bernal stacked. The micro-LEED patterns in Fig. 2(c) moreover show that within the grains, the layers are not misoriented/rotated relative to each other. A stacking with alternating 0 and 30° rotations of the layers relative to the SiC substrate, that decouples the layers,[3] is therefore neither plausible. Therefore, AA stacking seems the only available option left[39,40] for multilayer graphene showing linear dispersion at the $\bar{K}$ point, since Bernal (AB) and ABC stacking results in "hatlike" hyperbolic dispersions and split bands at the $\bar{K}$ point. A splitting of the π-bands from the different layers has also been predicted for AA stacking,[39,40] but this has not yet been possible to reveal or verify experimentally. Therefore, we speculate that the interaction and charge transfer between graphene layers grown on C-face SiC may be so weak/small that the band splitting is not resolvable in conventional ARPES where the probing area typically is fairly large so one integrates over many crystallographic grains. In XPEEM, one can collect PADs from a single grain, i.e., use a small enough probing area, and the highest energy resolution allow two bands that are split like the π-bands in Bernal stacked bilayer Si-face graphene to be resolved, see Fig. 1(e), but not closer lying bands. Nano-ARPES, which allow collection of spectra from individual grains using a considerably higher energy and momentum resolution,[45] could resolve closer lying bands and possibly provide some new insight into this puzzle concerning the π-band structure of single and multilayer C-face graphene. In a recent comparative theoretical study[46] of graphene grown on different SiC polytypes, where different buffer layer–graphene layer stackings were utilized, some intriguing results were reported. The Dirac bands in C-face graphene exhibited a vanishing band gap for all polytypes and for both AB and AA stacking, whereas in Si-face graphene, a splitting occurred for AB stacking but not for AA stacking. Since generally the interaction between graphene and substrate was reported[46] to be smaller on the C-face compared to the Si-face the splitting of the Dirac bands, if any, should be expected to be smaller on the C-face.

III. SUMMARY AND OUTLOOK

Our experimental results from graphene grown on nominally on-axis C-face SiC samples show the formation of fairly large (a few micrometer) grains of multilayer graphene, where adjacent layers are not rotated relative to each other, but that adjacent grains in general have different azimuthal orientations. This was concluded from the sharp (1×1) selected area LEED patterns observed and that only six Dirac cones centered around the $\bar{K}$ points in the

Brillouin zone appeared in the constant energy PAD patterns $E_i(k_x,k_y)$ recorded, using XPEEM, from different grains with 2–6 MLs of graphene. In LEED patterns collected at higher electron energy, diffraction spots from the SiC substrate were visible from 1- and 2-ML graphene areas and showed that the rotation angle between the graphene and the SiC substrate varied and was not always equal to 30° as for Si-face graphene. C 1*s* spectra collected from selected areas of 1, 2, 3, and 4 MLs of C-face graphene, respectively, did not show any hint of a carbon interface layer. Our findings are quite different compared to what other groups have reported earlier,[2,3,9,10,12,13,16–20] claiming rotational disorder between adjacent graphene layers on C-face SiC. We believe the main reason to be that the other groups had not succeeded to obtain grains of graphene large enough[7,8,16,17] to analyze the properties of individual grains.

A hydrogen treatment applied to C-face graphene samples was found to deteriorate the quality and properties of the graphene. The treatment drastically reduced the size of the graphene grains and the sample became sensitive to electron beam irradiation. An initial sharp (1×1) LEED pattern changed within minutes to a pattern containing strong superstructure spots, indicating the presence of twisted graphene layers. Local desorption of hydrogen from the graphene layers by the LEED electron beam was suggested as the cause, since an effect of electron beam exposure was clearly revealed by LEEM. These were quite unexpected findings, since hydrogen treatment has earlier been shown to have a positive effect on the properties of Si-face graphene.

Effects induced in the π-band structure around the $\overline{K}$ point after Na deposition and subsequent heating on a C-face graphene sample, with predominantly 2-ML coverage, were investigated. The Dirac point shifted after deposition away from the Fermi level, due to electron n-type doping. After heating at approximately 120–300 °C, the π-band appeared considerably broadened and collected core level spectra indicated Na intercalation between the graphene layers and at the interface. This broadening was therefore suggested to arise from two π-bands, shifted by a difference in doping concentration. PADs, $E_i(k_x,k_y)$ patterns, extracted from the clean C-face graphene sample looked very similar to earlier calculated distribution patterns for monolayer graphene and not Bernal stacked bilayer graphene. Also after Na deposition, the shape and intensity distribution of the patterns at energies below the Dirac point looked very similar, and at energies above the Dirac point, the patterns showed the flipped, "mirrored," intensity distribution predicted for monolayer graphene. Since selected area LEED and PADs show no rotational disorder between layers within a multilayer graphene grain, the earlier proposed special stacking model to decouple the layers[3] does not appear plausible. Therefore, AA stacking seems the only available option[39,40] for multilayer graphene showing linear dispersion at the $\bar{K}$ point, since AB and ABC stacking results in "hatlike" hyperbolic dispersions and split bands at the $\bar{K}$ point. A splitting of the π-bands is also predicted for AA stacked[39,40] multilayer graphene, but we speculate that the interaction between layers on C-face graphene may be so weak[46] that the band splitting is too small to be resolved in conventional ARPES where one typically integrates over many crystallographic grains. By XPEEM, one can at present only resolve bands with a splitting similar to the two π-bands in Bernal stacked bilayer Si-face graphene, as illustrated in Fig. 1(e). However, nano-ARPES could possibly[45] provide some new insight into this puzzle concerning the π-band structure of single and multilayer C-face graphene.

ACKNOWLEDGMENTS

The authors gratefully acknowledge support from the European Science Foundation, within the EuroGRAPHENE (EPIGRAT) program and the Swedish Research Council (Grant No. 621-2011-4252 and Linnaeus Grant).

REFERENCES

1. W. Lu, P. Soukiassian, and J. Boeckl: Graphene, fundamentals and functionalities. *MRS Bull.* **37**(12), 1119–1321 (2012).
2. P.N. First, W.A. de Heer, T. Seyller, C. Berger, J.A. Stroscio, and J.S. Moon: Epitaxial graphenes on silicon carbide. *MRS Bull.* **35**(4), 296 (2010).
3. M. Ruan, Y. Hu, Z. Guo, R. Dong, J. Palmer, J. Hankins, C. Berer, and W.A. de Heer: Epitaxial graphene on silicon carbide: Introduction to structured graphene. *MRS Bull.* **37**(12), 1138 (2012).
4. L.O. Nyakiti, V.D. Wheeler, N.Y. Garces, R.L. Myers-Ward, C.R. Eddy, Jr., and D.K. Gaskill: Enabling graphene-based technologies: Toward wafer-scale production of epitaxial graphene. *MRS Bull.* **37**(12), 1149 (2012).
5. C. Virojanadara, M. Syväjarvi, R. Yakimova, L.I. Johansson, A.A. Zakharov, and T. Balasubramanian: Homogeneous large-area graphene layer growth on 6H-SiC(0001). *Phys. Rev. B* **78**, 245403 (2008).
6. K.V. Emtsev, A. Bostwick, K. Horn, J. Jobst, G.L. Kellogg, L. Ley, J.L. McChesney, T. Ohta, S.A. Reshanov, J. Röhrl, E. Rotenberg, A.K. Schmid, D. Waldmann, H.B. Weber, and T. Seyller: Towards wafer-size graphene layers by atmospheric pressure graphitization of silicon carbide. *Nat. Mater.* **8**, 203 (2009).
7. C. Virojanadara, R. Yakimova, J.R. Osiecki, M. Syväjärvi, R.I.G. Uhrberg, L.I. Johansson, and A.A. Zakharov: Substrate orientation: A way towards higher quality monolayer graphene growth on 6H-SiC(0001). *Surf. Sci.* **603**, L87 (2009).
8. U. Starke, S. Forti, K.V. Emtsev, and C. Coletti: Engineering the electronic structure of epitaxial graphene by transfer doping and atomic intercalation. *MRS Bull.* **37**(12), 1177 (2012).
9. Luxmi, N. Srivastava, G. He, R.M. Feenstra, and P.J. Fisher: Comparison of graphene formation on C-face and Si-face SiC {0001} surfaces. *Phys. Rev. B* **82**, 235406 (2010).
10. C. Mathieu, N. Barrett, J. Rault, Y.Y. Mi, B. Zhang, W.A. de Heer, C. Berger, E.H. Conrad, and O. Renault: Microscopic correlation between chemical and electronic states in epitaxial graphene on SiC (000-1). *Phys. Rev. B* **83**, 235436 (2011).

11. L.I. Johansson, S. Watcharinyanon, A.A. Zakharov, T. Iakimov, R. Yakimova, and C. Virojanadara: The stacking of adjacent graphene layers grown on C-face SiC. *Phys. Rev. B.* **84**, 125405 (2011).
12. N. Srivastava, G. He, Luxmi, P.C. Mende, R.M. Feenstra, and Y. Sun: Graphene formed on SiC under various environments: Comparison of Si-face and C-face. *J. Phys. D: Appl. Phys.* **45**, 154001 (2012).
13. J. Hicks, K. Shepperd, F. Wang, and E.H. Conrad: The structure of graphene grown on the SiC(000-1) surface. *J. Phys. D: Appl. Phys.* **45**, 154002 (2012).
14. L.I. Johansson, C. Xia, J. Ul Hassan, T. Iakimov, A.A. Zakharov, S. Watchari-nyanon, R. Yakimova, E. Janzen, and C. Virojanadara: Is the registry between adjacent graphene layers grown on C-face SiC different compared to that on Si-face SiC. *Crystals* **3**, 1 (2013).
15. I. Forbeaux, J-M. Themlin, A. Charrier, F. Thibaudau, and J-M. Debever: Solid state graphitization mechanisms of silicon carbide 6H-SiC polar faces. *Appl. Surf. Sci.* **162–163**, 406 (2000).
16. J. Hass, R. Feng, J.E. Millan-Otoya, X. Li, M. Sprinkle, P.N. First, W.A. de Heer, E.H. Conrad, and C. Berger: Structural properties of the multilayer graphene/4H-SiC(000-1) system as determined by surface x-ray diffraction. *Phys. Rev. B* **75**, 214109 (2007).
17. J. Hass, F. Varchon, J.E. Millan-Otoya, M. Sprinkle, N. Sharma, W.A. de Heer, C. Berger, P.N. First, L. Magaud, and E.H. Conrad: Why multilayer graphene on 4H-SiC(000-1) behaves like a single sheet of graphene. *Phys. Rev. Lett.* **100**, 125504 (2008).
18. J. Hass, W.A. de Heer, and J. Conrad: The growth and morphology of epitaxial multilayer graphene. *J. Phys. Condens. Matter* **20**, 323202 (2008).
19. K.V. Emtsev, F. Speck, T. Seyller, L. Ley, and J.D. Riley: Interaction, growth, and ordering of epitaxial graphene on SiC {0001} surfaces: A comparative photoelectron spectroscopy study. *Phys. Rev. B* **77**, 155303 (2008).
20. M. Sprinkle, D. Siegel, Y. Hu, J. Hicks, A. Tejeda, A. Taleb-Ibrahimi, P. Le Fèvre, F. Bertran, S. Vizzini, H. Enriquez, S. Chiang, P. Soukiassian, C. Berger, W.A. de Heer, A. Lanzara, and E.H. Conrad: First direct observation of a nearly ideal graphene band structure. *Phys. Rev. Lett.* **103**, 226803 (2009).
21. D.L. Miller, K.D. Kubista, G.M. Rutter, M. Ruan, W.A. de Heer, P.N. First, and J.A. Stroscio: Structural analysis of multilayer graphene via atomic moire interferometry. *Phys. Rev. B* **81**, 125427 (2010).
22. T. Ohta, A. Bostwick, J.L. McChesney, T. Seyller, K. Horn, and E. Rotenberg: Interlayer interaction and electronic screening in multilayer graphene investigated with angle-resolved photoemission spectroscopy. *Phys. Rev. Lett.* **98**, 206802 (2007).
23. C. Riedl, C. Coletti, T. Iwasaki, A.A. Zakharov, and U. Starke: Quasi-free standing epitaxial graphene on SiC obtained by hydrogen intercalation. *Phys. Rev. Lett.* **103**, 246804 (2009).
24. C. Virojanadara, A.A. Zakharov, R. Yakimova, and L.I. Johansson: Buffer layer free large area bi-layer graphene on SiC(0001). *Surf. Sci.* **604**, L4 (2010).
25. S. Watcharinyanon, C. Virojanadara, J.R. Osiecki, A.A. Zakharov, R. Yakimova, R.I.G. Uhrberg, and L.I. Johansson: Hydrogen intercalation of graphene grown on 6H-SiC(0001). *Surf. Sci.* **605**, 1662 (2011).
26. S. Watcharinyanon, L.I. Johansson, C. Xia, and C. Virojanadara: Changes in structural and electronic properties of graphene grown on 6H-SiC(0001) by Na. *J. Appl. Phys.* **111**, 083711 (2012).
27. A. Sandin, T. Jayasekera, J.E. Rowe, K.W. Kim, M.B. Nardelli, and D.B. Dougherty: Multiple coexisting intercalation structures of sodium in epitaxial graphene-SiC interfaces. *Phys. Rev. B* **85**, 125410 (2012).
28. C. Xia, S. Watcharinyanon, A.A. Zakharov, L.I. Johansson, R. Yakimova, and C. Virojanadara: Detailed studies of Na intercalation on furnace grown graphene on 6H-SiC(0001). *Surf. Sci.* **613**, 88 (2013).
29. A. Bostwick, F. Speck, T. Seyller, K. Horn, M. Polini, R. Asgari, A.H. MacDonald, and E. Rotenberg: Observation of plasmarons in quasi-freestanding graphene. *Science* **328**, 999 (2010).
30. C. Virojanadara, S. Watcharinyanon, A.A. Zakharov, and L.I. Johansson: Epitaxial graphene on 6H-SiC(0001) and Li intercalation. *Phys. Rev. B* **82**, 205402 (2010).
31. C. Virojanadara, A.A. Zakharov, S. Watcharinyanon, R. Yakimova, and L.I. Johansson: A LEEM and XPEEM study of Li intercalated into graphene on SiC(0001). *New J. Phys.* **12**, 125015 (2010).
32. A.L. Walter, A. Bostwick, K-J. Jeon, F. Speck, M. Ostler, T. Seyller, L. Moreschini, Y.J. Chang, M. Polini, R. Asgari, A.H. MacDonald, K. Horn, and E. Rotenberg: Effective screening and plasmaron bands in graphene. *Phys. Rev. B* **84**, 085410 (2011).
33. S. Watcharinyanon, C. Virojanadara, and L.I. Johansson: Rb and Cs deposition on epitaxial graphene grown on 6H-SiC(0001). *Surf. Sci.* **605**, 1918 (2011).
34. D.A. Siegel, C.G. Hwang, A.W. Fedorov, and A. Lanzara: Quasifreestanding multilayer graphene films on the carbon face of SiC. *Phys. Rev. B* **81**, 241417 (2010).
35. L.I. Johansson, C. Xia, and C. Virojanadara: Na induced changes in the electronic band structure of graphene grown on C-face SiC. *Graphene* **2**, 1 (2013).
36. A.A. Zakharov, C. Virojanadara, S. Watcharinyanon, R. Yakimova, and L.I. Johansson: Nano-scale 3D(E, k_x, k_y) band structure imaging on graphene and intercalated graphene. *IBM J. Res. Dev.* **55**(4), 6 (2011).
37. H. Hibino, K. Kagashima, F. Maeda, M. Nagase, Y. Kobayashi, and H. Yamaguchi: Microscopic thickness determination of thin graphite films formed on SiC from quantized oscillation in reflectivity of low-energy electrons. *Phys. Rev. B* **77**, 075413 (2008).
38. L.I. Johansson, F. Owman, and P. Mårtensson: High-resolution core level study of 6H-SiC(0001). *Phys. Rev. B* **53**, 13793 (1996).
39. S. Latil, V. Meunier, and L. Henrard: Massless fermions in multilayer graphitic systems with misoriented layers: Ab initio calculations and experimental fingerprints. *Phys. Rev. B* **76**, 201402 (2007).
40. S. Latil and L. Henrard: Charge carriers in few-layer graphene films. *Phys. Rev. Lett.* **97**, 036803 (2006).
41. T. Ohta, T.E. Beechem, J.T. Robinson, and G.L. Kellogg: Long-range atomic ordering and variable interlayer interactions in two overlapping graphene lattices with stacking misorientations. *Phys. Rev. B* **85**, 075415 (2012).
42. J. Ul Hassan, C. Virojanadara, A. Meyer, I.G. Ivanov, J.I. Flege, S. Watcharinyanon, J. Falta, L.I. Johansson, and E. Janzén: Control of epitaxial graphene thickness on 4H-SiC(0001) and buffer layer removal through hydrogen intercalation. *Mater. Sci. Forum* **717–720**, 605 (2012).
43. M. Mucha-Kruczyński, O. Tsyplyatyev, A. Grishin, E. McCann, V.I. Fal'ko, A. Bostwick, and E. Rotenberg: Characterization of graphene through anisotropy of constant-energy maps in angle-resolved photoemission. *Phys. Rev. B* **77**, 195403 (2008).
44. I. Gierz, J. Henk, H. Hàchst, C.R. Ast, and K. Kern: Illuminating the dark corridor in graphene: Polarization dependence of angle-resolved photoemission spectroscopy on graphene. *Phys. Rev. B* **83**, 121408 (2011).
45. J. Avila, I. Razado, S. Lorcy, B. Lagarde, J-L. Giorgetta, F. Polack, and M.C. Asensio: ANTARES, a scanning photoemission microscopy beamline at SOLEIL. *J. Phys. Conf. Ser.* **425**, 192023 (2013).
46. O. Pankratov, S. Hensel, P. Gàtzfried, and M. Bockstedte: Graphene on cubic and hexagonal SiC: A comparative theoretical study. *Phys. Rev. B* **86**, 155432 (2012).